Journal of ELECTRONIC MATERIALS, Vol. 46, No. 1, 2017
DOI: 10.1007/s11664-016-4881-y

Correlation Between Microstructure and Optical Properties of Cu ($In_{0.7}$, $Ga_{0.3}$) Se_2 Grown by Electrodeposition Technique

ADEL CHIHI[1,2] and BRAHIM BESSAIS[1]

1.—Laboratoire photovoltaïque, Centre des recherches et des technologies de l'energie technopole Borj Cedria, B.P No 95, 2050 Hammam Lif, Tunisia. 2.—e-mail: supereagle2791@yahoo.fr

Polycrystalline thin films Cu ($In_{0.7}$, $Ga_{0.3}$) Se_2 (CIGSe) were grown on copper foils at various cathodic potentials by using an electrodeposition technique. Scanning electron microscopy showed that the average diameter of CIGSe grains increase from 0.1 μm to 1 μm when the cathodic potential decreases. The structure and surface morphology were investigated by x-ray diffraction and atomic force microscopy (AFM) techniques. This structure study shows that the thin films were well crystallized in a chalcopyrite structure without unwanted secondary phases with a preferred orientation along (112) plane. Energy-dispersive x-ray analyses confirms the existence of CIGSe single phase on a copper substrate. AFM analysis indicated that the root mean square roughness decreases from 64.28 to 27.42 when the potential deposition increases from −0.95 V to −0.77 V. Using Raman scattering spectroscopy, the A1 optical phonon mode was observed in 173 cm^{-1} and two other weak peaks were detected at 214 cm^{-1} and 225 cm^{-1} associated with the B2 and E modes of the CIGSe phase. Through spectroscopy ellipsometry analysis, a three-layer optical model was exploited to derive the optical properties and layer thickness of the CIGSe film by least-squares fitting the measured variation in polarization light versus the obtained microstructure.

Key words: CIGSe, electrodeposition, copper substrate, AFM, ellipsometry

INTRODUCTION

Copper indium gallium diselenide (CIGSe) is a remarkable I–III–VI_2 semiconductor for the development of second generation thin film solar cell devices. Indeed, CIGSe exhibits a combination of a large optical absorption coefficient of 10^5 cm^{-1}[1] and a direct optical band gap ranging from 1.05 eV to 1.73 eV by varying the In/Ga ratio, which is within the maximum solar absorption region,[2] and has high stability against photo-degradation. Besides the solar cell applications, CIGSe thin films can be used in transistor applications, like amorphous-silicon thin film transistors (TFTs),[3] and photoelectrodes in photoelectrochemical cells for hydrogen production.[4] Recently, laboratory-scale CIGSe deposited on a glass substrate for a 0.5-cm^2 device reached conversion efficiencies of about 21.7%,[5,6] which makes these types of semiconductor alloys very useful in large-area solar modules.[7] Zentrum for sonnenenergie-und wasserstoff-forschung (ZSW) is presently tackling the engineering challenge of transferring the latest high-efficiency processes to industrial in-line production equipment. Furthermore, CIGSe films can be deposited on flexible substrates,[8] where roll-to-roll processing allows high-throughput manufacturing. Up to now, CIGSe cells prepared on flexible metal substrates have achieved conversion efficiencies greater than 17%.[9] Several requirements, like light photovoltaic (LPV), and space power generation, can be realized using these flexible substrates.[10] Commonly, molybdenum (Mo) back contact is the most extensively used material owing to a good resistance temperature, and the ablity to customise an ohmic contact with CIGSe thin films.[11,12] However, Mo reacts with deposited CIGSe film to form a $MoSe_2$ interface, which acts as a barrier to the passage of the photo-

(Received March 11, 2016; accepted August 13, 2016; published online September 26, 2016)

generated carriers and accomplishes resistive losses within the solar cell.[13] Hence, te CIGSe/Mo structure converts to a CIGSe/$MoSe_2$/Mo structure.[14] In order to overcome this inconvenience, several studies have been carried out to improve the alternative back contact for CIGSe film. Copper foils have been used as an alternative to the Mo back contacts because of its considerable conductive material, which offers good ohmic contact with CIGSe films. These electrical characters allow the production of high-efficiency solar cells using a low-cost ohmic substrate and an optical reflector. Jo et al.[15] investigated the surface morphology of CIGSe films deposited on copper foils by pulsed laser deposition. They found that CIGSe crystallites are embedded in an amorphous copper-rich matrix and that the surface morphology is sensitive to surface temperature. Kampmann et al.[16] have deposited CIGSe films on copper foils by sequential plating of Cu, In and Ga species followed by Se evaporation, with yields of up to 9.0% cell efficiency. Moreover, they have established optical models with different compositions and thickness to calculate precisely the quantum efficiency of the cell device.[17,18] Nevertheless, to the best of our knowledge, these models do not refer to thicker samples and do not take microstructure into account.

In the present report, CIGSe thin films were electrodeposited on copper foils and characterized by using scanning electron microscopy (SEM), x-ray diffraction (XRD), energy-dispersive x-ray analyses (EDAX), Raman spectroscopy, atomic force microscopy (AFM), and spectroscopy ellipsometry (SE), with the main objective of correlating the microstructure of CIGSe films with optical properties such as refractive index n and extinction coefficient k to better understand the effect of film thickness and the role of microstructure in films features.

EXPERIMENTAL

Electrodeposition was achieved potentiostatically in a standard three-electrode electrochemical single-compartment cell without string at room temperature. The reference electrode was saturated calomel (SCE), the counter electrode was a platinum plate, and copper foil substrate (cathode) was used as the working electrode with a thickness of about 2.5 μm. In the first step, copper substrates were mirror-polished with sodium hydroxide (NaOH) crystals in warm water and rinsed with deionized water to remove the native oxide layer and adsorbed impurities. All copper foils substrates were smooth, uniform, and adherent. Then, a non-conductive scotch tape was applied on the back side of the copper substrate in order to avoid back surface deposition. Afterwards, deposition was carried out potentiostatically in an aqueous solution containing 6 mM ($CuCl_2(2H_2O)$), 4.5 mM ($InCl_3$), 0.75 mM (Ga_2O_3), 12 mM (SeO_2), and 0.1 M sodium citrate ($Na_3C_6H_5O_7$) which was chosen to be a complexing agent,[19,20] and 0.2 M lithium chloride (LiCl) was used as supporting electrolyte. The pH of the bath was adjusted to 2.15 using a high-purity dilute chlorhydric acid HCl (1 M) solution. The bath temperature was maintained at 25°C and kept without stirring during deposition. The solution was not deaerated before or during deposition. To assess different physical properties of the obtained layer, the cathodic potentials were varied from (−0.77 V) to (−0.95 V) versus SCE, which are suitable potentials for obtaining stable and controllable stoichiometry of CIGSe films.[21] As an optimized condition, the time of deposition was fixed at 10 min and the involved thicknesses were about 1.5 μm. Subsequently, CIGSe thin films were rinsed with deionized water and dried under a nitrogen flow at room temperature. Owing to the amorphous nature of the as-deposited films and in order to improve their crystallinity, all the films were annealed in an argon atmosphere at the optimized temperature of 400°C for 30 min. Finally, CIGSe films were characterized by SEM and EDAX, using an automated Bruker D8 advance x-ray diffraction spectrometer with CuKα radiations (λ = 1.541 Å) in the range of 2θ from 20° to 70°, Raman scattering with a helium–neon laser source with a wavelength of 632.81 nm was investigated using an AFM nanoscope III in tapping configuration mode to scan an area of 1 μm × 1 μm, and SE data were performed with a GES5 rotating polarizer spectroscopic ellipsometer over energy range from 1.54 eV to 4.13 eV with 0.01 eV resolution at the incidence angle 70°.

RESULTS AND DISCUSSION

Microstructure Analysis of the CIGSe Surface Films

The surface microstructure of the post-annealed CIGSe films on copper foil was investigated by SEM observations. As shown in Fig. 1a–c, micrographs of CIGSe samples are strongly affected by variation of cathodic potentials. It can be seen that all micrographs exhibit cauliflower-shaped morphology with non-uniform grain sizes and non-homogenous surfaces when the cathodic potential decreases from −0.77 V to −0.95 V versus SCE. The first CIGSe sample prepared at −0.77 V (Fig. 1a) displays densely packed, and small grain size of about 0.1 μm. Figure 1b exhibits particle-like morphology with inter-granular and voids for the 2nd film deposited at −0.85 V. For the third sample, Fig. 1c displays an increase in grain size of about 1 μm with polyhedral shape and lower porosity as compared to the two other samples. Commonly, cauliflower-shaped grains are indicative of the existence of a CIGSe chalcopyrite phase,[22] which proves the existence of the CIGSe chalcopyrite phase within the synthesized samples. Thus, the application of cathodic potential enabled us to grow CIGSe films

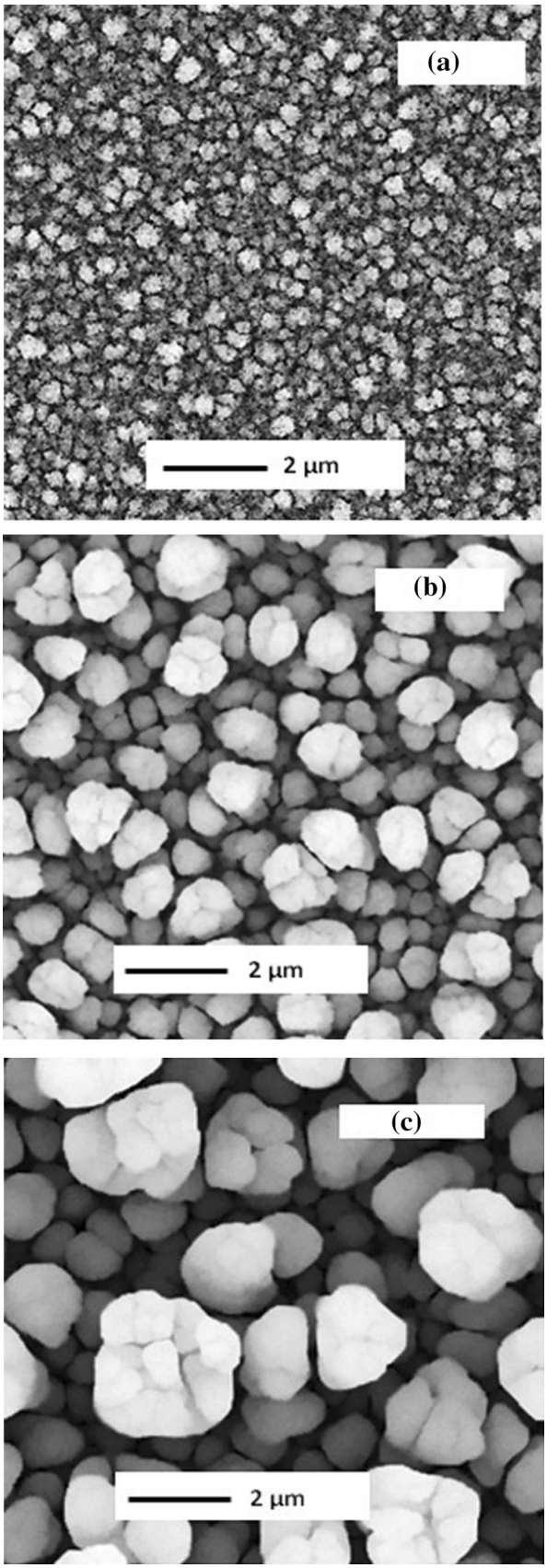

◀Fig. 1. SEM micrographs of CIGSe thin film deposited on a copper substrate at various cathodic potentials: (a) $E = -0.77$ V, (b) $E = -0.85$ V, (c) $E = 0.95$ V.

on a copper substrate with a controllable grain size. Similar results were obtained by using a radio frequency (RF) reactive magnetron co-sputtering technique and a co-evaporation technique with thermal crystallization of precursors in saturated selenium vapors.[23] For this result, we further investigated the existence of the CIGSe chalcopyrite phase for synthesized films in the following section.

Structural Characterization

To study the effect of the applied potential on the microstructure of the CIGSe samples, XRD is frequently the most suitable method. Figure 2 reveals the XRD patterns of CIGSe samples deposited from acidic baths with different cathodic potentials ranging from −0.77 V to −0.95 V versus SCE at an anodization time of 10 min on the copper foil substrate. All XRD patterns display characteristic peaks of the copper substrate JCPDS (Joint Committee of Powder Diffraction Standards) with card number (004-0836). It can be seen that, as the cathodic potentials decrease further, the copper intensity peak decreases considerably, which indicates the increasing of CIGSe thickness. On the other hand, the XRD patterns exhibit a prominent peak near $2\theta = 26.8°$ and two tiny peaks at 44.6° and 52.9°, which correspond to the (112), (220/204), and (312) reflection planes of the $Cu(Ga_{0.3}, In_{0.7})Se_2$ phase (JCPDS card File, 35-1102), respectively. Analysis of the patterns also reveals the nonexistence of a secondary crystalline phase like $Cu_{2-x}Se$. Therefore, the prepared CIGSe films crystallize well in the tetragonal chalcopyrite structure with a preferred orientation along the (112) plane. In order to further investigate the presence of the CIGSe chalcopyrite phase, EDAX analysis revealed atomic proportion ratios of Cu:In:Ga:Se of about 22.5:15.75:6.75:55.0 for all the samples, which confirms the XRD result. Moreover, quantitative information about the favored crystallite orientation has been obtained from the texture coefficient Tc $(h\ k\ l)$ along the appropriate diffraction plane. The different texture coefficients Tc $(h\ k\ l)$ were calculated for all the samples from XRD by the well-known equation[24]:

$$Tc(hkl) = \frac{I_{(hkl)}/I_{0(hkl)}}{\left(1/N\right)\sum_n I_{(hkl)}/I_{0(hkl)}} \qquad (1)$$

where I $(h\ k\ l)$ is the measured relative intensity of a plane $(h\ k\ l)$, I_0 $(h\ k\ l)$ is the matching recorded JCPDS data card intensity of the $(h\ k\ l)$ plane, N is

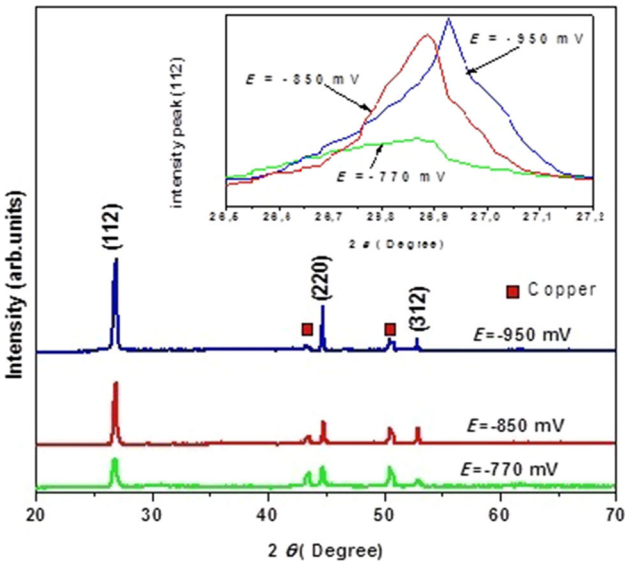

Fig. 2. X-ray diffraction patterns of electrodeposited CIGSe thin film at various cathodic potentials.

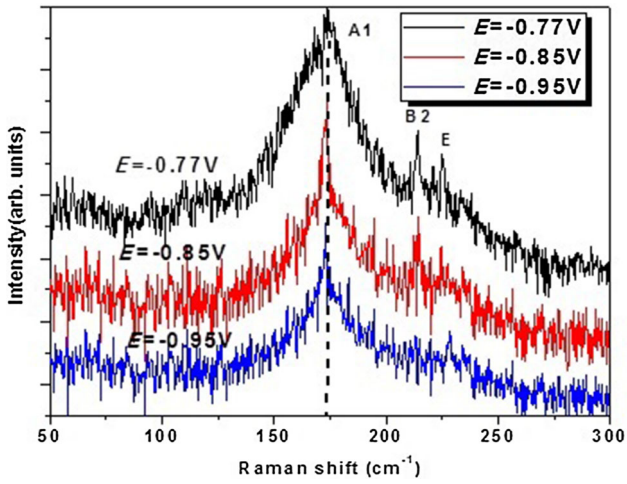

Fig. 3. Raman spectra of CIGSe samples on copper substrate with different cathodic potentials.

Table I. Effect of deposition potential on the preferred orientation of electrodeposited CIGSe thin films

Deposition potential (V)	(*h k l*)	*Tc* (*h k l*)
−0.77	(112)	0.67
	(220)	0.95
	(312)	1.37
−0.85	(112)	1.45
	(220)	0.86
	(312)	0.72
−0.95	(112)	1.72
	(220)	0.98
	(312)	1.28

Table II. XRD results obtained for electrodeposited CIGSe thin films through (112) orientation

Deposition potential (V)	Bragg angle 2θ (°)	Scherrer's crystallite size *D* (nm)
−0.77	26.5 ± 0.2	17 ± 2
−0.85	26.3 ± 0.2	28 ± 2
−0.95	26.9 ± 0.2	51 ± 2

the number of preferred directions of the growth, and n is the number of diffraction peaks considered in the analysis. The values of Tc (h k l) for different peaks of tetragonal chalcopyrite structure are listed in Table I. The highest value of Tc through the (112) plane is 1.72 for deposited film at −0.95 V. However, Tc is less to 1 towards the preferred orientation (112) plane for CIGSe film deposited at −0.77 V. This behavior could be explained by interdiffusion of the copper substrate in the deposited film, and for higher cathodic potential (−0.77 V), the Cu/(In+Ga) atomic ratio became greater than 1. Thereby, the copper-rich condition may block the growth of the (112) plane of the deposited CIGSe layer.[25] The copper diffusion from the substrate to the CIGSe film can affect the performance of the solar cells. On the other hand, we notice a small shift of the (112) peak to higher angles at the position 26.9° for the film deposited at the potential of −0.95 V versus SCE as shown in Fig. 2. The shift of the Bragg reflection peaks near the estimated stoichiometric compound (2θ = 26.8°, JCPDS card File, 35-1102) probably reveals the relief of stress in the CIGSe film, which leads to anisotropic deformation of the lattice. According to the literature, similar results were detected for CIGSe films on a copper foil substrate.[15] Nevertheless, CIGSe films deposited at potentials of −0.77 V and −0.85 V versus SCE display no shift of angle. Concerning the average crystallite size (D) of the Cu ($Ga_{0.3}$, $In_{0.7}$) Se_2 along the (112) plane was calculated by Debye–Scherrer's relationship[26]:

$$D = \frac{0.9\lambda}{\sqrt{\beta^2 - \beta_0^2}\cos\theta} \qquad (2)$$

where β is the full width at half-maximum (FWHM) of the diffraction peak located at 2θ expressed in radians, β_0 = 0.2° is the width of the matching peak due to the instrumental, and λ is the XRD wavelength (1.541 Å). Table II displays the average crystallite size of CIGSe films ranging from 17 nm to 51 nm when the cathodic potentials decrease from −0.77 V to −0.95 V versus SCE. These values are in good agreement with those obtained by Awasthi et al.[27] The inconsistency found in the values of grain sizes measured by XRD and those from SEM can be elucidated by taking into account that SEM measurements directly identify the surface morphology of the agglomerated grains, which

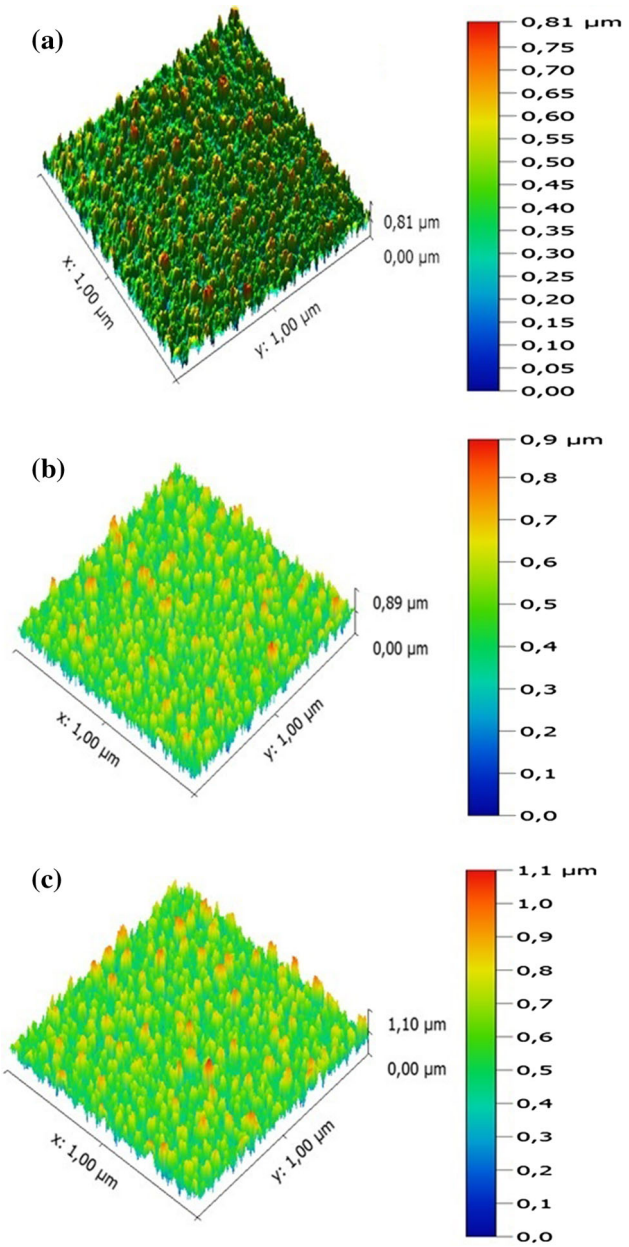

Fig. 4. 3D AFM micrographs of CIGSe thin films on a copper substrate with various cathodic potentials: (a) $E = -0.77$ V, (b) $E = -0.85$ V, (c) $E = -0.95$ V.

delivers the particle size. The later results show that the obtained crystallite sizes are two times better than those achieved by pulsed laser deposition.[15] This enhancement of crystallite size is suitable for solar cell applications.

Raman Spectra of CIGSe Films

To confirm the results obtained by XRD and SEM, we used the Raman technique spectroscopy, which can determine the vibration modes of CIGSe thin films. Figure 3 exhibits the Raman spectra recorded at room temperature by a helium–neon laser (632.81 nm) from the frequency range of 50–300 cm^{-1}. According to the selection rules of Raman scattering, the signal detected at 173 cm^{-1} is close to the A1 optical phonon mode which is specific to the chalcopyrite structure[28] and two other weak peaks detected at 214 cm^{-1} and 225 cm^{-1} are associated with the B2 and E modes of the CIGSe phase.[29,30] In spite of the A1 mode present in the whole samples, the intensity and contrast peak varies, which means that the films have non-uniformity on the surface. Moreover, the $Cu_{2-x}Se$ phase impurities were not detected in the range of 260–275 cm^{-1}, which is in agreement with the XRD results. Matching the literature, similar results were found in CIGSe thin films deposited onto Mo-coated soda-lime glass substrates by radio frequency reactive magnetron sputtering.[31]

Atomic Force Microscopy Measurements

AFM is a versatile tool that allows the imaging of topography and the characterization of CIGSe surfaces such as morphology, surface roughness, grain size, uniformity, and so on. We use this technique to estimate the thickness as well the root mean square (RMS). The AFM was exploited in tapping mode to scan an area of 1 μm × 1 μm. All the three-dimensional (3D) AFM micrographs, the RMS, and the grain size were performed by using Gwyddion free software v.2.43 developed by Czech metrology.[32] Figure 4 depicts 3D AFM micrographs of three CIGSe thin films at various cathodic potentials. As shown in the AFM micrographs, the surface morphology iis strongly dependent on different cathodic potentials. Additionally, all CIGSe films exhibited distributed areas with elongated grains randomly oriented and hollow areas with diverse roughness. The RMS roughness R_q value can be expressed using the following equation:

$$R_q = \sqrt{\frac{1}{N}\sum_{j=1}^{N}(Z_j - \tilde{Z})^2} \quad (3)$$

where N, Z_j, and $\tilde{Z}$ are the total number of height measurements, every height value, and the mean height, respectively. The value of RMS roughness increases from 27.42 ± 0.13 nm to 64.28 ± 0.13 nm when the potential deposition decreases from −0.77 V to −0.95 V, as shown in Table III. The increase in cathodic potential signals an improvement in the surface layer indicating the decrease in RMS roughness, which is crucial for the production a high-quality solar cell.[33]

Ellipsometric Studies

In order to investigate the effect of potential deposition on the optical properties, we took the SE data to reveal the film thickness and dielectric function of the studied model as shown in Fig. 5. The SE technique was used to measure Ψ and Δ ellipsometric parameters over a wavelength ranging

Table III. The estimated RMS surface roughness by AFM measurements

Potential deposition (V)	RMS roughness (nm)
−0.77	27.42 ± 0.13
−0.85	43.12 ± 0.13
−0.95	64.28 ± 0.13

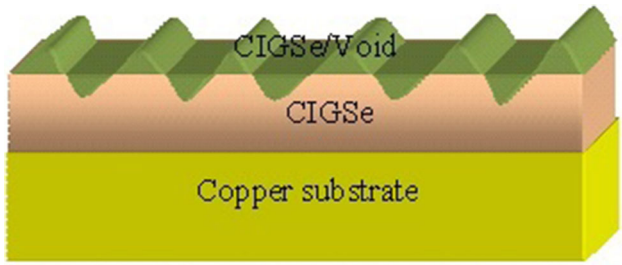

Fig. 5. A three-layer optical model used throughout the ellipsometry study.

from 400 nm to 1200 nm at the incidence angle 70°. Ψ and Δ represent the amplitude ratio and phase difference of the incident and reflected light waves, respectively. These ellipsometric parameters involve the ratio of the complex Fresnel coefficients r_P and r_S, representing the reflected light polarized in parallel component (P) and the perpendicular component (S) relative to the incident plane, respectively.[34]

$$\rho = \frac{r_p}{r_s} = \tan\Psi \exp j\Delta \tag{4}$$

An optical three-layer model (Fig. 5) was used for the copper foil substrate with an infinite thickness, the CIGSe layer of thickness d_s, and a top roughness layer of thickness d_r. The dielectric function of the roughness layer was established from the Bruggeman effective medium approximation (BEMA) composed of a mixture of the underlying CIGSe bulk layer and voids[35] as follows:

$$f_{CIGSe}\frac{\varepsilon_{CIGSe}-\varepsilon_{eff}}{\varepsilon_{CIGSe}+2\varepsilon_{eff}} + f_v\frac{\varepsilon_v-\varepsilon_{eff}}{\varepsilon_v+2\varepsilon_{eff}} = 0 \tag{5}$$

$$f_{CIGSe} + f_v = 1 \tag{6}$$

where ε_{CIGSe} denotes the dielectric functions of CIGSe layer, ε_v is the dielectric functions of voids, ε_{eff} is the effective dielectric function of the mixture and f_{CIGSe} and f_v represent the volume fractions of averaged grains of CIGSe and voids, respectively. In order to acquire the optical properties of the CIGSe layer, a complex dielectric function was modeled by the Tauc–Lorentz dispersion formula. Jessison and Modine[36] have exhibited the imaginary dielectric function as follows:

$$\varepsilon_i(E) = \begin{cases} 0 & \text{for } E \le Eg \\ \frac{1}{E}\frac{AE_0C(E-E_g)^2}{(E^2-E_0^2)^2+C^2E^2} & \text{for } E > Eg \end{cases} \tag{7}$$

The real part of the dielectric function ε_r is calculated by the Kramers–Kronig integration:

$$\varepsilon_r(E) = \varepsilon_r(\infty) + \frac{2}{\pi}P\int_{E_g}^{\infty}\frac{\xi\epsilon_i(\xi)}{\xi^2-E^2}d\xi \tag{8}$$

where P is the Cauchy principal value containing the residues of the integral located on the lower half of the complex plane and along the real axis. A, C, E_0, E_g and $\varepsilon_r(\infty)$ refer to the amplitude, broadening term of energy, peak central energy, optical gap energy, andf high-frequency dielectric constant, respectively. All the parameters were fitted with origin software as shown in Table IV. The Levenberg–Marquardt algorithm (LMA), a non-linear least-squares method, is exploited for the modeling. The root means square error (RMSE) χ can be acquired by the following equation[37]:

$$\chi = \sqrt{\frac{1}{2n-N-1}\sum_{j=1}^{n}\left(\left(\tan\psi_j^{exp}-\tan\psi_j^{th}\right)^2+\left(\cos\Delta_j^{exp}-\cos\Delta_j^{th}\right)^2\right)} \tag{9}$$

where n is the number of measured Ψ and Δ pairs integrated into the fit, N is the number of fit parameters, $\tan\Psi^{th}$ and $\cos\Delta^{th}$ are the theoretical values, and $\tan\Psi^{exp}$ and $\cos\Delta^{exp}$ are the measured values. Figure 6a and b displays the calculated values of Ψ and Δ and the experimental SE data by using the parameters of the Tauc–Lorentz dispersion formula. It can be seen from Fig. 6 that the good fit of the experimental data is due to the small value of RMSE, which projected the accuracy of the used model for the estimation of the optical properties of the CIGSe films.

The assessments of optical parameters of CIGSe film, i.e. the refractive index n and the extinction coefficient k film, were deduced from Eqs. 7 and 8 by using the following relationships:

$$n = \sqrt{\frac{\left(\varepsilon_i^2+\varepsilon_r^2\right)}{2}} \tag{10}$$

$$k = \sqrt{-\varepsilon_i + \frac{\left(\varepsilon_i^2+\varepsilon_r^2\right)}{2}} \tag{11}$$

Figure 7 exhibits the fit and experimental refractive index. As can be seen, the gradual increase of refractive index with decreasing the applied cathodic potential from −0.77 V to −0.95 V (increasing film thickness) can be attributed to the increase in

Table IV. Thickness, RMSE, and fitted parameters of CIGSe films deposited at various potentials derived by using the Tauc–Lorentz dispersion model

Potential deposition (V)	Thickness (nm)	RMSE	A	C	E_0(eV)	Eg (eV)	$\varepsilon_r(\infty)$
−0.77	854 ± 5	2	24	2.4	2.238	1.42 ± 0.05	3.231 ± 0.024
−0.85	965 ± 5	9	65	3.5	2.554	1.38 ± 0.05	3.231 ± 0.024
−0.95	1100 ± 5	13	114	4.1	3.187	1.24 ± 0.05	3.231 ± 0.024

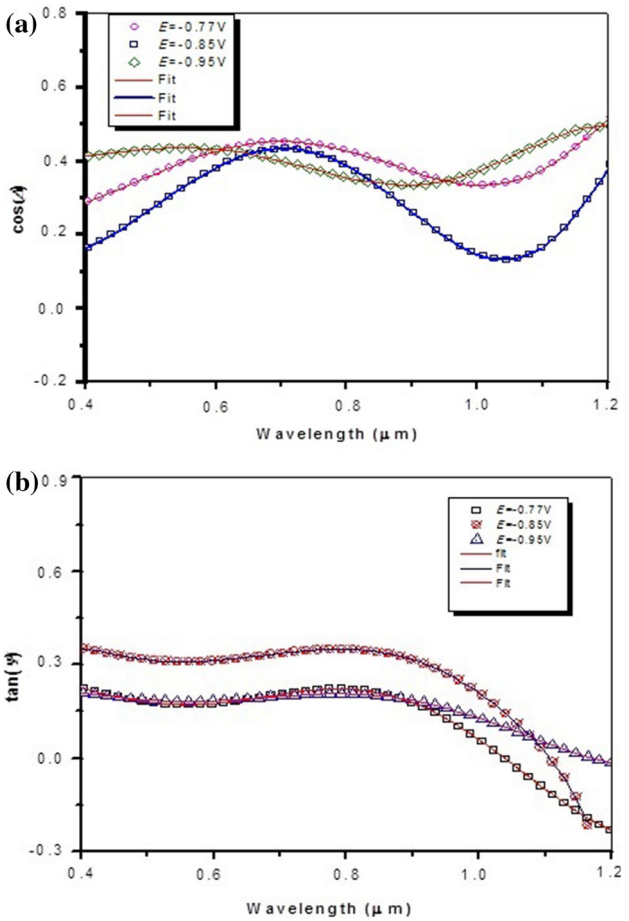

Fig. 6. The fitted experimental (a) cosΔ and (b) tanΨ, spectra of electrodeposited CIGSe thin films on a copper substrate for various cathodic potentials.

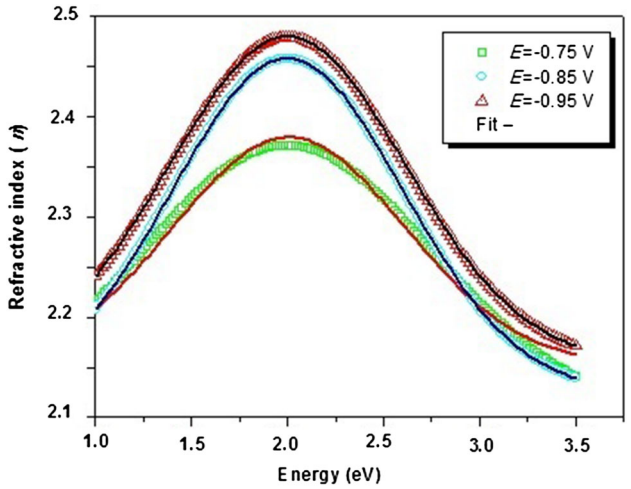

Fig. 7. The fitted experimental refractive index as a function of energy of electrodeposited CIGSe thin films on a copper substrate for various cathodic potentials.

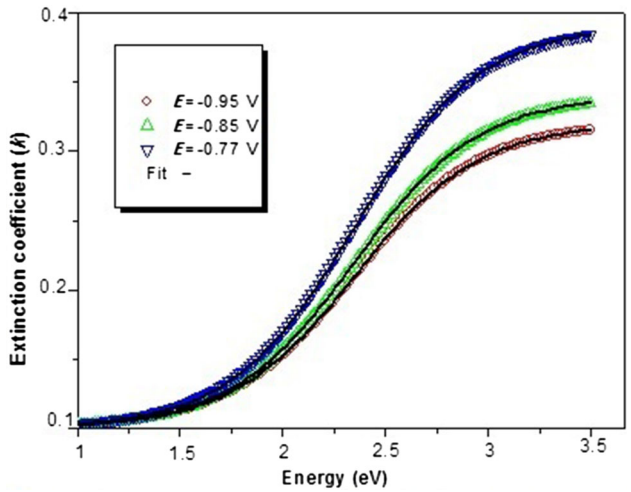

Fig. 8. The fitted experimental extinction coefficient as a function of energy of electrodeposited CIGSe thin films on a copper substrate for various cathodic potentials.

the packing density and/or the composition fluctuations caused by the variation of distribution grain size. The samples with large grains (lower cathodic potential), a rough surface and fewer voids displays slightly higher n values while the rest have lower n values owing to smaller grains, accompanied by large number of tiny voids in the film, and to little surface roughness. On the other hand, the extinction coefficient is considerably affected by the variation of potential deposition as shown in Fig. 8. As can be seen, the experimental data of the extinction coefficient are in good agreement with our theoretical model taking into account the low calculated values of RMSE. In the infrared region, i.e. below 1.25 eV, the extinction coefficient tails of all the samples display a slight variation, but not equal to zero, which indicate short optical losses and intrinsic contributions owing to grain size disorder in the synthesized layer. Analogous extinction coefficient tails have also been previously reported by using the ellipsometry analysis of

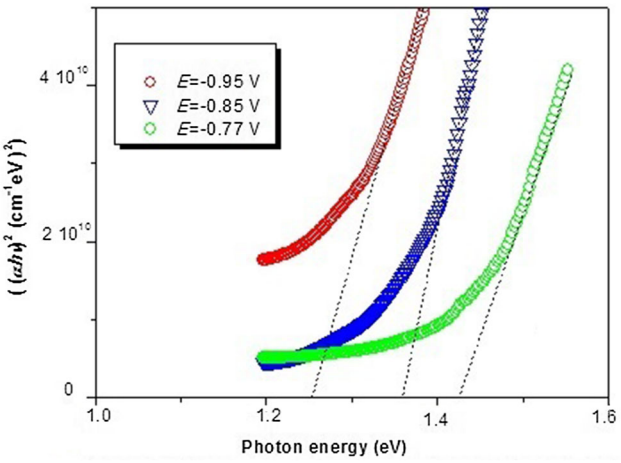

Fig. 9. $(\alpha h\nu)^2$ against incident photon energy of electrodeposited CIGSe thin films on a copper substrate for various cathodic potentials.

CIASe thin films.[38] However, in the visible ranges, i.e. between 1.55 eV and 3.1 eV, the extinction coefficient increases with the rising of incident photon energy of all the films. The optical constants established for the CIGSe layer on the copper foil substrate are approximately similar with those reported by Paulson et al.[39,40] In order to understand the nature of the transition on the basis of the dependence of the absorption coefficient with the incident photon energy $h\upsilon$ and according to the Beer–Lambert law, the absorption coefficient α $(h\nu)$ of CIGSe films can be determined from the values of the extinction coefficients k and λ by using the following relationship $\alpha = \frac{4\pi k}{\lambda}$. Consequently, the energy band gaps can be estimated by extrapolating the linear region of the curve $(\alpha h\nu)^2$ to the intercept of the horizontal axis $h\nu$ according to the Tauc's relationship.[41] The estimated optical band gap decreases from 1.42 eV to 1.24 eV as the cathodic potential decreases from −0.77 V to −0.95 V, as shown in Fig. 9. It is noted that the higher energy band gap was associated with higher cathodic potential (−0.77 V) and so to smaller grain size. The shift of the energy band gap with grain size was also investigated in terms of the density of states model suggested by Mott et al.[42] They proposed that chalcopyrite films usually have a large number of unsaturated bonds or defects, which create localized states in the energy band gap. Thus, when the cathodic potential further increases, the unsaturated defects are gradually decreasing, which causes a blue shift of the energy band gap. Such behavior is quite essential for considering CIGSe films on a copper substrate as suitable absorbers for solar cell applications. As provided by AFM and XRD studies, the ellipsometric results confirm the impact of the cathodic potential in the microstructure and optical properties.

CONCLUSION

In summary, we have investigated the effect of the potential deposition at room temperature on the microstructure characteristics and surface composition of CIGSe thin films grown by an electrodeposition technique on copper foil. SEM, XRD, EDAX, and Raman technique spectroscopy confirms that the films annealed at the optimized temperatureof 400°C for 30 min are mainly formed by the Cu ($In_{0.7}$, $Ga_{0.3}$) Se_2 polycrystalline chalcopyrite phase. The RMS surface roughness of the deposited CIGSe film was found to increase from 27.42 nm to 64.28 nm with the decrease of potential deposition. The optical properties and CIGSe films thickness were determined by means of SE measurements in terms of three-layer optical model. The type of optical transition responsible for optical absorption is direct transitions. The obtained values from the fitting graphs show that optical band gaps are affected by the microstructure.

ACKNOWLEDGEMENTS

We are grateful to photovoltaic laboratory (LPV) of the research and technology center of energy (CRTEn), technopole of Borj Cedria. Tunisia.

REFERENCES

1. F. Kang, J. Ao, G. Sun, Q. He, and Y. Sun, *J. Alloys Compd.* 478, L25 (2009).
2. G. Hanna, A. Jasenek, U. Rau, and H.W. Schock, *Thin Solid Films* 387, 71 (2001).
3. X. Zhu and C.W. Liu, *Appl. Phys. Lett.* 105, 143502 (2014).
4. R.C. Valderrama, P.J. Sebastian, J.P. Enriquez, and S.A. Gamboa, *Sol. Energy Mat. Sol. Cells* 88, 145 (2005).
5. P. Jackson, D. Hariskos, E. Lotter, S. Paetel, R. Wuerz, R. Menner, W. Wischmann, and M. Powalla, *Prog. Photovolt. Res. Appl.* 19, 894 (2011).
6. P. Jackson, D. Hariskos, R. Wuerz, O. Kiowski, A. Bauer, T.M. Friedlmeier, and M. Powalla, *Phys. Status Solidi RRL* 9, 28 (2015).
7. M. Powalla, M. Cemernjak, J. Eberhardt, F. Kessler, R. Kniese, H.D. Mohring, and B. Dimmler, *Sol. Energy Mater. Sol. Cells* 90, 3158 (2006).
8. K. Orgassa, H.W. Schock, and J.H. Werner, *Thin Solid Films* 431–432, 387 (2003).
9. M. Powalla, W. Witte, P. Jackson, S. Paetel, E. Lotter, R. Wuerz, F. Kessler, C. Tschamber, W. Hempel, D. Hariskos, R. Menner, A. Bauer, S. Spiering, E. Ahlswede, T.M. Friedlmeier, D. Blazquez-Sanchez, I. Klugius, and W. Wischmann, *IEEE J. Photovolt.* 4, 440 (2014).
10. B.M. Başol, V.K. Kapur, C.R. Leidholm, A. Halani, and K. Gledhill, *Sol. Energy Mat. Sol. Cells* 43, 93 (1996).
11. P. Chelvanathan, Z. Zakaria, Y. Yusoff, M. Akhtaruzzaman, M.M. Alam, M.A. Alghoul, K. Sopian, and N. Amin, *Appl. Surf. Sci.* 334, 129 (2015).
12. T. Wada, N. Kohara, S. Nishiwaki, and T. Negami, *Thin Solid Films* 387, 118 (2001).
13. Y.C. Lin, M.T. Shen, Y.L. Chen, H.R. Hsu, and C.H. Wu, *Thin Solid Films* 570, 166 (2014).
14. H. Mirhosseini, J. Kiss, G. Roma, and C. Felser, *Thin Solid Films* 606, 143 (2016).
15. Y.H. Jo, B.C. Mohanty, and Y.S. Cho, *Appl. Surf. Sci.* 256, 6819 (2010).
16. A. Kampmann, J. Rechid, A. Raitzig, S. Wulff, M. Mihhailova, R. Thyen, and K. Kalberlah, *MRS Proc.* 763, B8.5 (2003).
17. S. Sunkoju, S. Schujman, D. Dixit, A. Diebold, J. Li, R. Collins, and P. Haldar, *Thin Solid Films* 606, 113 (2016).

18. J. Claypoole, B. Peace, N. Sun, D. Dwyer, M.D. Eisaman, P. Haldar, and H. Efstathiadis, *J. Alloys Compd.* 657, 873 (2016).
19. S. Aksu, J. Wang, and B.M. Basol, *Electrochem. Solid State Lett.* 12, D33 (2009).
20. C. Su, W. Ho, H. Lin, C. Nieh, and S.C. Liang, *Sol. Energy Mater. Sol. Cells* 95, 261 (2011).
21. Y. Lai, F. Liu, Z. Zhang, J. Liu, Y. Li, S. Kuang, J. Li, and Y. Liu, *Electrochim. Acta* 54, 3004 (2009).
22. H.K. Song, J.K. Jeonga, H.J. Kim, S.K. Kim, and K.H. Yoon, *Thin Solid Films* 435, 186 (2003).
23. J. Gao, W. Jie, Y. Yuan, T. Wang, G. Zha, and J. Tong, *J. Vac. Sci. Technol. A* 29, 051507 (2011).
24. L. Fanni, B.A. Aebersold, D.T.L. Alexander, L. Ding, M.M. Masis, S. Nicolay, and C. Ballif, *Thin Solid Films* 565, 1 (2014).
25. P.K. Mishra, J.N. Prasad, V. Dave, R. Chandra, and A.K. Choudhary, *Mater. Sci. Semicond. Process.* 34, 350 (2015).
26. B.D. Cullity and S.R. Stock, *Elements of X-Ray Diffraction*, 3rd ed. (Upper Saddle River: Prentice Hall, 2001).
27. V. Awasthi, S.K. Pandey, S.K. Pandey, S. Verma, M. Gupta, and S. Mukherjee, *J. Mater. Sci. Mater. Electron.* 25, 3069 (2014).
28. J. Olejníček, C.A. Kamler, A. Mirasano, A.L. Martinez-Skinner, M.A. Ingersoll, C.L. Exstrom, S.A. Darveau, J.L. Huguenin-Love, M. Diaz, N.J. Ianno, and R.J. Soukup, *Sol. Energy Mater. Sol. Cells* 94, 8 (2010).
29. S. Roy, P. Guha, S.N. Kundu, H. Hanzawa, S. Chaudhuri, and A.K. Pal, *Mater. Chem. Phys.* 73, 24 (2002).
30. K. Kondo, H. Sano, and K. Sato, *Thin Solid Films* 326, 83 (1998).
31. T. Jia, L. Dong, Z. Zhao, X. Li, and D. Li, *Surf. Coat. Tech.* 259, 94 (2014).
32. P. Klapetek, D. NeČas, and C. Anderson, *Gwyddion Software User Guide*, Version 2.45 (Czech Metrology Institute, 2009), http://www.cmi.cz, http://gwyddion.net/.
33. A.M. Hermann, M. Mansour, V. Badri, B. Pinkhasov, C. Gonzales, F. Fickett, M.E. Calixto, P.J. Sebastian, C.H. Marshall, and T.J. Gillespie, *Thin Solid Films* 361–362, 74 (2000).
34. R.M.A. Azzam and N.M. Bashara, *Ellipsometry and Polarized Light* (Amsterdam: North Holland, 1977).
35. D.A.G. Bridgeman, *Ann. Phys.* 24, 636 (1935).
36. G.E. Jellison and F.A. Modine, *Appl. Phys. Lett.* 69, 371 (1996).
37. C. Talagrand, X. Boddaert, D.G. Selmeczi, C. Defranoux, and P. Collot, *Thin Solid Films* 590, 134 (2015).
38. M.I. Alonso, M. Garriga, C.A.D. Rincon, and M. Leon, *J. Appl. Phys.* 88, 5796 (2000).
39. P.D. Paulson, R.W. Birkmire, and W.N. Shafarman, *J. Appl. Phys.* 94, 879 (2003).
40. S. Theodoropoulou, D. Papadimitriou, K. Anestou, Ch. Cobet, and N. Esser, *Semicond. Sci. Technol.* 24, 015014 (2009).
41. J.H. Lee, X. Ke, N.J. Podraza, L.F. Kourkoutis, T. Heeg, M. Roeckerath, J.W. Freeland, C.J. Fennice, J. Schubert, D.A. Muller, P. Schiffer, and D.G. Schlom, *Appl. Phys. Lett.* 94, 212510 (2009).
42. N.F. Mott and E.A. Davis, *Electronic Processes in Non-Crystalline Materials* (Oxford: Clarendon Press, 1979), p. 210.